

See discussions, stats, and author profiles for this publication at:  
<https://www.researchgate.net/publication/228476999>

# Excited states and gas phase photofragmentation of palladium and platinum hexafluoroacetylacetonates

ARTICLE *in* COORDINATION CHEMISTRY REVIEWS · OCTOBER 2000

Impact Factor: 12.24 · DOI: 10.1016/S0010-8545(00)00356-8

---

CITATIONS

10

---

READS

9

3 AUTHORS, INCLUDING:



Jeffrey I Zink

University of California, Los Angeles

470 PUBLICATIONS 22,143 CITATIONS

SEE PROFILE

# Excited states and gas phase photofragmentation of palladium and platinum hexafluoroacetylacetonates

Peter Muraoka, Daniel Byun, Jeffrey I. Zink \*

*Department of Chemistry and Biochemistry, University of California, Los Angeles, CA 90095, USA*

Received 14 October 1999; accepted 10 March 2000

## Contents

Abstract . . . . .	194
1. Introduction . . . . .	194
2. Electronic spectra and assignments in condensed media . . . . .	196
2.1 Absorption and emission spectra . . . . .	196
2.2 Molecular orbital calculations and assignments of the electronic spectra . . . . .	196
2.2.1 Pd(acac) <sub>2</sub> . . . . .	196
2.2.2 Pt(acac) <sub>2</sub> . . . . .	197
2.3 Experimental studies of hexafluoroacetylacetonate complexes . . . . .	198
2.3.1 Ligand centered luminescence . . . . .	198
2.3.2 Single crystal spectra of Pt(hfac) <sub>2</sub> . . . . .	199
2.4 General observations . . . . .	200
3. Gas phase spectroscopy . . . . .	200
3.1 Absorption spectra . . . . .	200
3.2 Excitation spectra of Pt(hfac) <sub>2</sub> . . . . .	201
3.2.1 Assignments of the excitation bands . . . . .	202
3.2.2 Excited state geometry . . . . .	203
3.2.3 Comparisons between condensed media and gas phase spectra . . . . .	203
4. Gas phase photochemistry . . . . .	204
4.1 Solid photoproducts and metal CVD . . . . .	204
4.2 Identification of photoproducts by luminescence spectroscopy . . . . .	205
4.2.1 Atoms . . . . .	205
4.2.2 Metal-containing molecular fragments . . . . .	206
4.3 Mass spectroscopic identification of photofragments . . . . .	206
4.3.1 PdC wavelength dependence . . . . .	208

\* Corresponding author. Tel.: +1-310-8251001; fax: +1-310-2069880.

*E-mail address:* zink@chem.ucla.edu (J.I. Zink).

5. Summary . . . . .	209
Acknowledgements . . . . .	210
References . . . . .	210

---

## Abstract

The properties of excited electronic states of acetylacetonate complexes of palladium and platinum, and the photochemical reactivities of the fluorinated derivatives in the gas phase are reviewed. These complexes are precursors for the thermal and photochemical production of metal films via metal organic chemical vapor deposition. This review is organized in three sections. First, the electronic structure is surveyed, the results of molecular orbital calculations are discussed, and the theoretical results are compared with the electronic spectra. Second, gas phase spectroscopy is discussed. Both electronic absorption spectra of hot gases and excitation spectra in a molecular beam have been used to assign the lowest excited states. Finally, the gas phase photochemistry is discussed. Solid photoproducts including particles and films are briefly reviewed, and photoproducts in the gas (identified by emission and time of flight mass spectroscopy) are discussed. The relevance of the gas phase photochemistry to laser assisted chemical vapor deposition is emphasized. © 2000 Elsevier Science S.A. All rights reserved.

**Keywords:** Palladium; Platinum; Acetylacetonate ligands; Spectroscopy; Luminescence; Photochemistry; Photofragmentation; Chemical vapor deposition

---

## 1. Introduction

The utility of metal  $\beta$ -diketonate complexes as precursors for the thermal and photochemical production of metal films via metal organic chemical vapor deposition (CVD) has stimulated and renewed interest in the electronic properties and photochemical decomposition pathways of these complexes [1–5]. The fluorinated acetylacetonate ligands, especially (1,1,1,5,5,5-hexafluoro-2,4-pentanedionate = hfac, Fig. 1), provide good precursor volatility and allow for facile transport in the gas phase, but they may also result in fluorine and/or carbon contamination of the final deposit [6]. The unsubstituted ligand, and ligands with hydrocarbon substituents, have also been used, but the volatility is lower. Palladium and platinum acetylacetonate and substituted acetylacetonate complexes have been used as precursors for depositing thin films using both thermal (pyrolytic) and laser-assisted (photolytic) CVD. Films of these metals have potential applications as catalysts and as electrical contacts in microelectronics [7–11]. However, only recently have the gas phase photofragmentation processes of these compounds begun to be investigated.

Studies of the luminescence that is observed when metal-containing molecules are photolyzed under photochemically driven CVD conditions have shown that diatomic metal-containing molecules and metal atoms are produced in the gas phase [1–5,12–15]. These discoveries have assisted in the elucidation of the photolytic

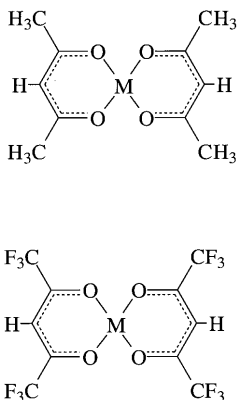


Fig. 1. Square-planar metal acac and hfac complexes.

decomposition pathways. Both desired fragments (e.g. TiN in the laser CVD of TiN films) [12] and undesirable fragments containing heteroatoms that contaminate the final films (e.g. CuF, CrF, NiF, PtC and PdC in the laser CVD of the respective metal films using the metal hfac precursor) [2–5,13,14] have been identified. In the case of the Pd and Pt hfac complexes, only the MC diatomic has been identified. Luminescence spectroscopic studies of Pt(hfac)<sub>2</sub> under LCVD conditions showed that diatomic PtC was produced in the gas phase, and time of flight mass spectroscopy showed that PdC is formed during the photolysis of Pd(hfac)<sub>2</sub>.

Gas phase spectroscopic and photochemical studies of this class of compounds have been limited in scope. Several studies have examined the processes leading to metal deposition from a precursor originating in the gas phase but only as it relates to its pyrolysis via local heating of the substrate by the laser [16–19]. Most of the investigations did not attempt to study the gas phase photolytic contributions to the process at the molecular level even though understanding these contributions will play a vital role in controlling the desired properties of the deposited film [9].

This review of spectroscopic and gas phase photochemical studies of Pd(II) and Pt(II)  $\beta$ -diketonates is organized in three sections. In the first section, the electronic structure of this class of metal complexes is surveyed. The results of molecular orbital calculations are discussed, especially with regard to the assignment of electronic states. Because the results of the theoretical calculations were compared with the electronic spectra obtained in condensed media, these spectroscopic results are also included. In the second section, gas phase spectroscopy is discussed. Electronic absorption spectra of hot gases have been measured, and excitation spectra of Pd(hfac)<sub>2</sub> (monitored by light emission) have been used to assign the lowest excited states. In the third section, the gas phase photochemistry is discussed. Solid products including particles and films are briefly reviewed. Photoproducts in the gas phase have been identified by using both emission spectroscopy and time of flight mass spectroscopy. A type of spectroscopy that has rarely been applied to transition metal complexes, resonance enhanced multiphoton ionization (REMPI)

spectroscopy, has been used to obtain highly resolved action spectra of both the palladium and platinum complexes. The insight obtained about photofragmentation pathways relevant to LCVD from the mass selected REMPI spectra is reviewed.

## 2. Electronic spectra and assignments in condensed media

The electronic absorption spectroscopy and assignments of the transitions of square-planar  $\beta$ -diketonate complexes of Pd(II) and Pt(II) have a long and complex history. In the earliest studies of the Group 10 complexes, the low energy bands of the Ni(II) complex were assigned to ligand field transitions and the lowest allowed transition assigned to two nearly-degenerate  $\pi\pi^*$  transitions [20]. However, the spectra of the Pd and Pt complexes were described as more complex and were not assigned. Subsequent to these early studies, both experimental and theoretical research has continued, but a consensus about the assignments and electronic structure still has not been reached.

Among the complicating features that result in difficulties in making assignments are the effects of axial interactions (e.g. interactions with the solvent), solvatochromism (i.e. shifts in band energies as a function of the dielectric constant of the medium), and the highly mixed nature of the closely spaced excited states (dd, MLCT, LMCT, and ligand localized  $\pi\pi^*$ ). Molecular orbital calculations are helpful in identifying the mixing, but the calculations are based on isolated molecules (appropriate for the gas phase) although the comparison spectra are obtained in condensed media where the solvent effects can be appreciable.

In this section we review recent results on the electronic spectra and electronic structure of Pd(II) and Pt(II)  $\beta$ -diketonates. We focus on the spectra in condensed media; the gas phase results are discussed in the following sections.

### 2.1. Absorption and emission spectra

The absorption spectra band maxima and molar absorptivities of Pd and Pt acetylacetonate and hexafluoroacetylacetonate complexes are summarized in Table 1. A large number of complexes containing substituted acac ligands have also been studied [21–23], but only the parent acac and hfac complexes will be discussed here. Both the Pd and the Pt hfac complexes are luminescent at low temperatures. The emission maxima and band widths are listed at the bottom of Table 1. Note that the emission spectra have maxima in the red region of the visible spectrum and extend into the near IR.

### 2.2. Molecular orbital calculations and assignments of the electronic spectra

#### 2.2.1. $Pd(acac)_2$

Molecular orbital calculations using ZINDO (INDO/S-SCF-CI) [21], PSHONDO [24], and DV Xa [25] have been reported. The ZINDO and DV Xa

Table 1  
Reported band maxima (nm) and molar absorptivities ( $M^{-1} \text{ cm}^{-1}$ ) for Pd and Pt complexes

Pd(acac) <sub>2</sub> <sup>21</sup>		Pt(acac) <sub>2</sub> <sup>21</sup>	
Band max.	$\epsilon$	Band max	$\epsilon$
380	(sh)	344	$3.9 \times 10^3$
326	$9.8 \times 10^3$	286	$7.9 \times 10^3$
250	(sh)	252	$1.1 \times 10^4$
228	$2.5 \times 10^4$	226	$1.2 \times 10^4$
Pd(hfac) <sub>2</sub> <sup>23</sup>		Pt(acac) <sub>2</sub> <sup>22</sup> (single crystal)	
Band max.	$\epsilon$	Band max.	FWHM
408	$6.2 \times 10^2$	400	$4000 \text{ cm}^{-1}$
357	$4.9 \times 10^3$		
333	$3.4 \times 10^4$		
246	$1.1 \times 10^4$		
227	$3.2 \times 10^4$		
<i>Emission</i> Pd(hfac) <sub>2</sub> <sup>a</sup>		Pt(acac) <sub>2</sub> <sup>22</sup> (single crystal)	
Band max.	FWHM	Band max.	FWHM
724	$2500 \text{ cm}^{-1}$	666	$4000 \text{ cm}^{-1}$

<sup>a</sup> This work.

methods provide a similar ordering and energy separation of the three highest occupied orbitals, with the next three molecular orbitals bunched at similar energies. The methods also provide similar descriptions of the bonding for the highest occupied MOs [21].

The two lowest excited singlet states according to the ZINDO calculation are mixtures of metal dd, ligand  $\pi\pi^*$  and ligand-to-metal charge transfer (LMCT) transitions [21]. The lowest state (calculated at 377 nm) is primarily dd and ligand oxygen to  $d_{xy}$  in character; the  $\pi\pi^*$  component was 18%. The next lowest state, at 332 nm, is 76% ligand  $\pi$  to metal  $d_{xy}$  in character, and 23% dd. The next highest state at 329 nm is nearly pure  $\pi\pi^*$ .

### 2.2.2. *Pt(acac)<sub>2</sub>*

Molecular orbital calculations based on PSHONDO have been reported [24]. (ZINDO calculations were not carried out because of limitations in the parameterization schemes [21].) These studies focused on the occupied frontier orbitals and compared the results with photoelectron spectra. The energy order of the three highest occupied orbitals of Pt was calculated to be the same as that for Pd. Small differences in population analyses as well as some changes in the energy sequence of some of the MOs were found. The Pt–O overlap populations showed that there

are stronger metal–ligand  $\sigma$  and  $\pi$  interactions in the Pt complex than in the Pd complex. For example, the  $d_{xz}$  contribution to the HOMO in  $\text{Pt}(\text{acac})_2$  is double that calculated for  $\text{Pd}(\text{acac})_2$ . The bonding and non-bonding MOs were stabilized and the antibonding MOs destabilized in Pt versus Pd.

### 2.3. Experimental studies of hexafluoroacetylacetonate complexes

More detailed electronic spectra have been reported for the hfac complexes than for the acac complexes, but the level of detail in the MO calculations is lacking. In the case of the hfac complexes, luminescence spectroscopy has been used to identify the position of the  $\pi\pi^*$  transition in the ligand (which is relatively insensitive to the nature of the metal) and the lowest energy LMCT band in the Pd complex.

#### 2.3.1. Ligand centered luminescence

The position of the lowest energy emission is almost independent of the metal and was assigned by using complexes with filled d shells (e.g.  $\text{Zn}(\text{II})$ ,  $\text{Au}(\text{III})$ ,  $\text{Al}(\text{III})$ ) [13,26]. This independence suggests the transition is ligand centered and is assigned to a  $\pi\pi^*$  transition. A combination of luminescence spectroscopy, resonance Raman spectroscopy and time-dependent theory support this assignment. For example, the resonance Raman spectra show highly displaced modes that are all ligand centered, as discussed below. The emission spectra of solid samples of  $\text{Zn}(\text{hfac})_2 \cdot 2\text{H}_2\text{O}$ ,  $\text{Me}_2\text{Au}(\text{tfac})$ ,  $\text{Me}_2\text{Au}(\text{acac})$  and  $\text{Al}(\text{acac})_3$  were measured at 18 K.

The emission spectra of the two non-fluorinated acetylacetonate compounds have similar onset energies of  $25\,000\text{ cm}^{-1}$ . The full width at half maximum (FWHM) of the two bands are also very similar ( $\sim 3500\text{ cm}^{-1}$ ). The spectrum of  $\text{Al}(\text{acac})_3$  consists of a single broad band, whereas that of the  $\text{Me}_2\text{Au}(\text{acac})$  compound contains resolved vibronic structure with the main progression consisting of a spacing of about  $1350\text{ cm}^{-1}$ . The emission spectrum of  $\text{Me}_2\text{Au}(\text{tfac})$  has an  $E_{00}$  of about  $23\,000\text{ cm}^{-1}$  and a FWHM of about  $4000\text{ cm}^{-1}$ . The spectrum has resolved vibronic structure with the main progression consisting of a  $1352\text{ cm}^{-1}$  spacing, similar to that in the  $\text{Me}_2\text{Au}(\text{acac})$  spectrum. The emission spectrum of  $\text{Zn}(\text{hfac})_2 \cdot 2\text{H}_2\text{O}$  has an  $E_{00}$  value of  $22\,500\text{ cm}^{-1}$  with a FWHM of  $2200\text{ cm}^{-1}$ . This emission spectrum from this compound is the most resolved of those studied. The two main progressions in the spectrum are created by a low-energy mode of  $262\text{ cm}^{-1}$  and a high-energy mode of  $1352\text{ cm}^{-1}$ .

These emission spectra of the  $\beta$ -diketonate complexes are assigned to the ligand centered  $\pi^*$  to  $\pi$  transition. For a given ligand, the energy of the emission is not very sensitive to the metal. In the case of the hfac complexes, almost no change in  $E_{00}$  is observed when the metal is changed from gold to zinc. In the case of the acac complexes, changing the metal from gold to aluminum only changes the value of  $E_{00}$  by  $700\text{ cm}^{-1}$ . The onset of the emission bands moves only slightly in energy with changes in the fluorine content in the acetylacetonate ligand. The acac compounds emit at a slightly higher energy than the tfac compound, and the tfac compound emits at slightly higher energy than the hfac compounds. These small shifts are caused by the perturbations on the  $\pi$  orbital energies by the substituent

$\text{CF}_3$  groups. A similar trend was reported for the energies of the spin allowed  $\pi-\pi^*$  absorption bands of iron(III) complexes [27].

Resonance Raman spectroscopy was also used to assist in the assignments. The vibrational normal modes that are most strongly resonance enhanced are those undergoing the largest distortions as a result of the electronic transition. The only active modes in the emission spectra are ligand centered modes. In the resonance Raman spectrum of  $\text{Zn}(\text{hfac})_2 \cdot 2\text{H}_2\text{O}$ , the peak at  $1352\text{ cm}^{-1}$  corresponding to the mixed C–C and C– $\text{CF}_3$  stretches is the most intense band in the spectrum. Other bands having intensities of greater than 5% of that of the most intense band are the C=C stretch, the CO stretch, the C– $\text{CF}_3$  stretch and a  $262\text{ cm}^{-1}$  ring deformation mode [28–31]. All of these modes are localized on the  $\beta$ -diketonate ligand and the resonance Raman results support the  $\pi^*$  to  $\pi$  assignment. The changes in the normal coordinates were calculated quantitatively by using the resonance Raman intensities, the electronic spectra, and time-dependent theory [26].

### 2.3.2. Single crystal spectra of $\text{Pt}(\text{hfac})_2$

The absorption and emission spectra of a single crystal of  $\text{Pt}(\text{hfac})_2$  at 77 K have been reported [20]. The spectra are shown in Fig. 2. The absorption spectrum consists of a broad peak with a maximum at  $25\,000\text{ cm}^{-1}$ , a width at half-height of  $4000\text{ cm}^{-1}$ , and almost no vibronic fine structure. The spectrum in a cyclohexane solution at room temperature also contains a broad band at about  $23\,000\text{ cm}^{-1}$  with a molar absorptivity of  $>10^3\text{ M}^{-1}\text{ cm}^{-1}$ . This band contains poorly resolved vibronic bands at about  $22\,010$ ,  $23\,100$  and  $24\,200\text{ cm}^{-1}$ . A weaker band is found to lower energy at  $22\,000\text{ cm}^{-1}$ .

The single crystal emission spectrum at 77 K is shown on the left side of Fig. 2. The bandwidth at  $4000\text{ cm}^{-1}$  is about the same as that of the single crystal absorption band. The onset of the emission band overlaps that of the absorption band at about  $19\,000\text{ cm}^{-1}$ . Poorly resolved vibronic fine structure is observed with an energy spacing of  $1400\text{ cm}^{-1}$ .

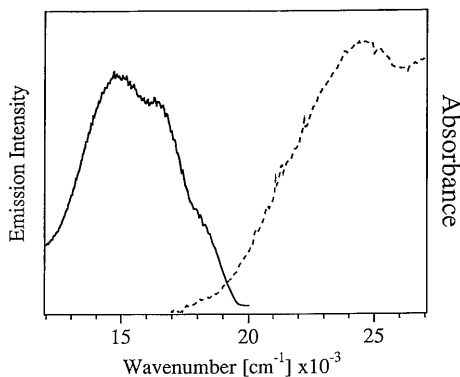


Fig. 2. Single crystal emission spectra at 20 K (solid line) and absorption spectra at 77 K (dashed line). The emission was excited at 364 nm.



The lowest energy absorption and corresponding emission bands in the crystal were assigned to a LMCT transition. The bands overlap and have about the same width. However, the relative energies of the ligand field and the LMCT states change as a function of the medium surrounding the molecule. Details of these changes and their origins are discussed in the next section.

#### 2.4. General observations

The picture that emerges from the experimental studies and from the molecular orbital calculations is complicated and incomplete, but several general conclusions can be drawn. First, the excited states in the  $\beta$ -diketonate complexes are strongly mixed and (with the possible exception of the ligand centered  $\pi\pi^*$  state), it is not meaningful to assign single labels to the states. The  $\pi\pi^*$  state in hfac complexes has its origin between 22 000 and 23 000  $\text{cm}^{-1}$  for molecules in condensed media; states having mixed dd and charge transfer character lie to lower energy in the case of Pd and Pt complexes. The relative positions of the lowest states having predominantly dd character and LMCT character are dependent on the medium and switch positions in the  $\text{Pt}(\text{hfac})_2$  complex between the crystal and the gas phases.

### 3. Gas phase spectroscopy

The energy orderings of excited states of molecules in the gas phase may be different from those in condensed media. Thus, the gas phase spectroscopic properties of a molecule must be measured and understood; it may be misleading to rely on solution phase assignments. Effects such as inhomogeneous broadening are absent for isolated molecules in the gas phase and more highly resolved spectra may be obtained. Two experiments that elucidate the gas phase spectroscopic properties of  $\text{Pd}(\text{hfac})_2$  and  $\text{Pt}(\text{hfac})_2$  have been reported: absorption spectroscopy of both molecules in a hot gas, and excitation spectroscopy of  $\text{Pt}(\text{hfac})_2$  in a cold collision-free molecular beam.

#### 3.1. Absorption spectra

The gas phase absorption spectrum of  $\text{Pt}(\text{hfac})_2$  has been reported [8]. The absorption maximum occurs at 257 nm with a molar absorptivity on the order of  $10^4 \text{ M}^{-1} \text{ cm}^{-1}$ . A set of bands corresponding to the LMCT excited state ( $\epsilon > 10^3 \text{ M}^{-1} \text{ cm}^{-1}$ ) occurs around 400 nm and weaker features that are assigned to spin-allowed ligand field transitions occur around 500 nm ( $\epsilon > 10^3 \text{ M}^{-1} \text{ cm}^{-1}$ ). These bands are similar to those observed in the solution phase absorption spectra taken in cyclohexane solution, but the LMCT state in the gas phase is blue-shifted by about 30 nm. The ligand field bands lie lower than the LMCT bands in both the gas phase and in the poorly coordinating solvent due to weak axial interactions with other molecules. These interactions become evident in the single crystal

absorption spectra where the ligand field bands now lie higher in energy than the LMCT state. The solvent effects on the absorption spectra will be discussed in the following section.

The absorption spectrum of  $\text{Pd}(\text{hfac})_2$  obtained from a hot gas exhibits similar structure to that of  $\text{Pt}(\text{hfac})_2$ . The  $\text{Pd}(\text{hfac})_2$  spectrum shows the same structure with slightly stronger absorbencies and a shift of 25 nm to shorter wavelengths [7]. The absorption spectra of these complexes is relevant to the discussion of the excitation spectra that are discussed in the following sections.

The above assignments of the bands observed in the gas phase absorption spectra are consistent with the molar absorptivities, but use the simplifying assumptions that the states are not strongly mixed. The molecular orbital calculations discussed in Section 2 suggests that the states are highly mixed. However, the theory does not accurately calculate the energies or the order of the states observed in the gas phase. In the following discussion, the language of the simplifying assumptions will be used, although it should be kept in mind that there is some degree of mixing. The assignments based on the absorption spectra are verified by the more highly resolved excitation spectra that are discussed next.

### 3.2. Excitation spectra of $\text{Pt}(\text{hfac})_2$

Excitation spectra of  $\text{Pt}(\text{hfac})_2$  in the gas phase have been reported [22]. The spectra were obtained by measuring the emission intensity as a function of the excitation wavelength. The excitation spectra contain resolved vibronic structure. Detailed knowledge of the geometry changes that occur in molecular excited states was obtained [22]. In order to use electronic spectroscopy to measure distortions along the many normal coordinates that may be displaced, resolution must be sufficiently high to observe individual vibronic components of the absorption or emission band. Inhomogeneous broadening of spectra obtained in condensed media obscures the desired vibronic bands and only a smooth, broad envelope is observed. To minimize the effects of condensed media, the spectra were obtained under the collision free conditions in a supersonic molecular beam.

The excitation spectrum was recorded between 22 000 and 26 000  $\text{cm}^{-1}$  and is shown in Fig. 3. The lowest energy feature is a broad band with very little resolved structure. Its onset occurs at about 21 000  $\text{cm}^{-1}$  and its maximum is at 21 900  $\text{cm}^{-1}$ . The higher energy region of the spectrum is dominated by a set of three sharper bands with maxima at 22 700, 23 985 and 25 400  $\text{cm}^{-1}$ . These bands, with an average separation of 1350  $\text{cm}^{-1}$ , contain resolved fine structure. Smaller features containing structure are observed between the three sharp, intense bands.

The magnified spectrum in the region between 22 500 and 23 500  $\text{cm}^{-1}$  containing the first of the intense, sharp bands as well as some of the smaller features is shown in Fig. 4. The vibronic fine structure on the most intense band is evident in the expanded spectrum. The vibronic bands are not well resolved, but a regular spacing between the shoulders of 65  $\text{cm}^{-1}$  is found. The vibronic structure in the less intense band in Fig. 4 is even less well resolved, but the same energy spacing is evident.

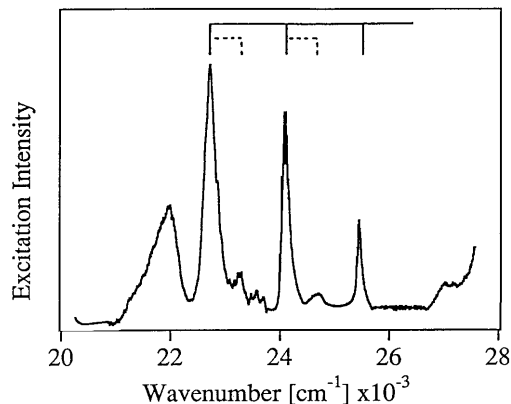


Fig. 3. Excitation spectra of  $\text{Pt}(\text{hfac})_2$  in a supersonic molecular beam. The solid and dotted lines on the top of the spectrum indicate the progressions in the  $1350$  and  $597\text{ cm}^{-1}$  modes, respectively.

### 3.2.1. Assignments of the excitation bands

The bands observed in the excitation spectra of  $\text{Pt}(\text{hfac})_2$  in the molecular beam are assigned to transitions to two electronic states: a low lying ligand field excited state and a slightly higher energy LMCT excited state. The weak features arise from vibronic structure. The prominent series of sharp intense bands at  $22\,700$ ,  $23\,985$  and  $25\,400\text{ cm}^{-1}$  are assigned to vibronic components of the LMCT state. The weak bands  $597\text{ cm}^{-1}$  to higher energy from each of these bands are assigned to additional vibronic components of the LMCT state.

The vibronic peaks in the molecular beam excitation spectrum are assigned by comparison with the electronic ground state vibrations of the molecule and of

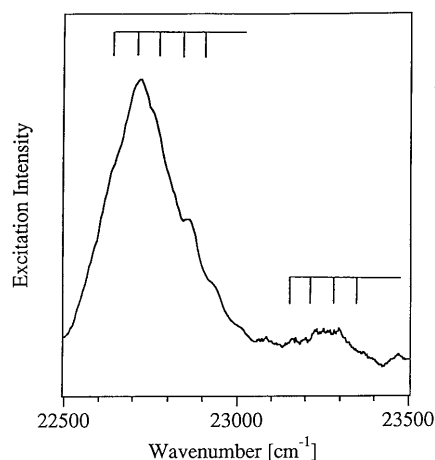


Fig. 4. Expanded view of the excitation spectra of  $\text{Pt}(\text{hfac})_2$  in a supersonic molecular beam in the region between  $22\,500$  and  $23\,500\text{ cm}^{-1}$ . The progression in the  $65\text{ cm}^{-1}$  mode is indicated on top.

analogous complexes [32–34]. The three prominent peaks separated by  $1350\text{ cm}^{-1}$  are assigned the mixed C–C and C–CF<sub>3</sub> stretching mode. The smaller peaks that are  $597\text{ cm}^{-1}$  higher in energy from the sharp peaks in the molecular beam spectrum are assigned to a quantum of the Pt–O totally symmetric stretch. The structure on the above peaks with a separation of  $65\text{ cm}^{-1}$  arises from a progression in a totally symmetric ring deformation mode. Distortions in these modes are expected in transitions that involve the  $\pi$  system on the ligand and a metal d orbital involved in Pt–O bonding.

### 3.2.2. Excited state geometry

The intensities of the vibronic transition in the spectral region  $22\,500\text{--}26\,000\text{ cm}^{-1}$  were quantitatively analyzed. Time-dependent theory is used to calculate the spectrum from the multidimensional potential surfaces of the initial and final states [22,35,36]. The major changes are in the metal–ligand Pt–O bond and in the C–O and C–C bonds in the ring with the largest change occurring in the C–O bond. Bond length changes in Pt–O and C–O were calculated to be  $0.011$  and  $0.023\text{ \AA}$ , respectively. The O–Pt–O bond angle change is  $2.0^\circ$ . These values were calculated using coupled potential surfaces.

### 3.2.3. Comparisons between condensed media and gas phase spectra

The measurement of the LMCT-state energy from isolated molecules in the gas phase enables comparisons to be made between the gas phase and condensed media [22]. The LMCT band observed from isolated molecules in the molecular beam excitation spectrum is blue shifted relative to the absorption band obtained in condensed media. When the environment is changed from cyclohexane to the beam, a blue shift of the first vibronic peak of  $600\text{ cm}^{-1}$  is observed. The shift is small but significant, especially since cyclohexane is often assumed to have very weak effects on the spectra of solutes because it is a non-polar, non-coordinating solvent. The shift of the LMCT band when the medium is changed from the crystal to the molecular beam is  $>1000\text{ cm}^{-1}$ .

The relative energies of the ligand field and the LMCT states change as a function of the medium of the molecule. In isolated molecules in the molecular beam, the lowest energy band is assigned as a ligand field transition. The ligand field band is also lowest in energy in the hot gas spectrum [37] and in the cyclohexane solution spectrum. On the other hand, the lowest energy band in the crystal is the LMCT band. The observed band energy changes were attributed to the change in the energy of the ligand field excited state as a function of axial interactions. In the crystal, axial interactions with other molecules raise the energy of the ligand field band higher than that of the LMCT band. In the gas phase and in the poorly coordinating solvent, axial interactions are weak and the ligand field band lies lower than the LMCT state. In addition, the LMCT state blue shifts by more than  $1000\text{ cm}^{-1}$  from the condensed media to the gas-phase. Both of these effects combine to give the observed ordering of the states.

#### 4. Gas phase photochemistry

Photochemical reactions of molecules in the gas phase may be very different from those in solution. The most important differences are the absence of a solvent cage, the absence of solvent molecules as reactants and the absence of specific solvent interactions. In addition, when reactions are studied under collision-free conditions, the electronic state that is populated is usually the origin of the reaction or the luminescence; vibrational relaxation by collisions does not occur. Thus, wavelength-dependent photochemistry is the rule rather than the exception. Finally, multiphoton events are common. Multiphoton absorption, either sequentially or coherently, delivers a large amount of energy to the molecule. The result may be photofragmentation of the original molecule resulting in photoproducts ranging from the molecular ion down to bare atoms. Useful photoproducts such as solid particles or patterned films can be obtained. In this section, gas phase photoreactions of  $\text{Pd}(\text{hfac})_2$  and  $\text{Pt}(\text{hfac})_2$  are reviewed.

##### 4.1. Solid photoproducts and metal CVD

Highly dispersed Pd, Pt, and bimetallic Pd/Pt powders with varying stoichiometric compositions are formed from  $\text{Pd}(\text{hfac})_2$  and  $\text{Pt}(\text{hfac})_2$  via 248 nm excimer laser excitation in the gas phase [11]. According to the authors, the photodissociation process is due to single photon absorption. By varying the flow rate of each carrier gas independently, the Pd:Pt ratio in the powders changes. Particle sizes range from 1 to 3 nm. The total metal content in the bimetallic powders is between 7–10%, while the carbon content is  $55 \pm 5\%$ . The carbon arises from the photolytic fragments of the parent molecule to form larger particles (100 nm) that serve as support material for the smaller metal particles. These results show that clusters can be formed by photolysis entirely in the gas phase and not due to any thermal reactions caused by surface heating by the laser.

Platinum deposition from  $\text{Pt}(\text{hfac})_2$  and its wavelength dependence has been reported [8]. These aspects were studied in conjunction with varying laser power and laser beam diameter, but only with respect to the deposition rate and not with respect to the purity of the resulting deposit. Both gas phase and surface reactions were studied, but only the gas phase results will be reviewed here. The study was performed at four different wavelengths (257, 334, 363 and 454 nm) corresponding to four different absorption peaks in the UV–vis absorption spectra of  $\text{Pt}(\text{hfac})_2$ . There is a low power regime (0.001–0.2 mW) in which the deposition rate increases, a higher power regime (0.2–5 mW) in which the deposition rate decreases due to desorption of the surface adlayer, followed by another increase in deposition rate above 5 mW due to gas-phase photolysis. The point at which the deposition rate starts to decrease with increasing laser power is at lower power with decreasing wavelength. Similarly, the point at which the deposition rate starts to increase again due to gas phase photolysis occurs at lower power for shorter wavelengths.

A ‘saturation’ of the gas-phase photolytic deposition rate occurs at the longer wavelengths. The authors proposed that the gas phase photodecomposition at these

conditions ( $\lambda = 454$  nm) is actually an incoherent sequential two-photon process [8]. The intermediate state that results upon the absorption of the first photon can diffuse out of the laser beam prior to being decomposed by a second photon. In addition, it may undergo other processes such as internal conversion, which makes it unavailable for dissociation by absorption of the second photon.

The deposition rate depends on the molar absorptivity  $\varepsilon$  of  $\text{Pt}(\text{hfac})_2$ . A general trend of increasing LCVD rate is observed with increasing  $\varepsilon$ . A relative measure of efficiency defined by the ratio  $r = \varepsilon/\text{LCVD rate}$  shows that the dissociation efficiency is smallest at 514 and 488 nm. These wavelengths are associated with the same transition. It is also noted that although  $\varepsilon(488 \text{ nm}) = \varepsilon(477 \text{ nm})$ , the LCVD rate and therefore  $r$  is twice as high at 477 nm because the two wavelengths may be involved in different transitions. In the case where the changes in  $\varepsilon$  are substantial (477, 467, 454 nm) however, the values for  $r$  are identical and the absorption spectra suggest that the wavelengths excite the same transition. A constant  $r$  value is found at lower wavelengths (363, 351, and 334 nm) for the same reason, but although the energy of photons increases by 30%, the relative efficiency of dissociation decreases by 25%. This suggests that excitation near 460 nm involves a channeling of some excitation events into non-dissociating pathways.

An estimate of the absolute magnitude of the relative photodissociation efficiencies was also calculated. The photodissociation efficiency in the gas phase ( $\phi_g =$  number of atoms deposited per second divided by the number of photons absorbed per second) at  $\lambda = 350$  nm increases from 1.5 to  $4 \times 10^{-2}$  when the laser power is increased from 10 to 30 mW.  $\phi_g$  does not increase with the transmitted light intensity, suggesting the existence of a competing mechanism such as collisional deactivation of the intermediate state, diffusion of the intermediate state out of the laser beam, or losses by some other process. In addition, the gas phase photolytic deposition rate increases with precursor vapor pressure and laser power and decreases with increasing beam diameter. The slope of the LCVD rate versus power plot is nearly 2 for gas-phase photolysis, implying that the rate-determining step is a two-photon process.

#### 4.2. Identification of photoproducts by luminescence spectroscopy

Luminescence of atoms and small metal containing molecules is observed upon laser irradiation and can be used to identify the photofragments resulting from laser photolysis [1,12–15]. In this section, the spectra and the identification of fragments that contain a metal are reviewed. Many metal-free fragments (e.g. CH,  $\text{C}_2$ ) have been observed, but the emphasis in this section is on the metal and metal-containing molecular fragments.

##### 4.2.1. Atoms

The production of metal atoms resulting from the multiphoton dissociation of organometallic molecules in the gas phase is well known [38]. Multiple photon fragmentation is not normally observed in the condensed phase due to a loss of excess internal energy to the surrounding medium prior to dissociation. The

presence of bare metal atoms has been observed by emission from electronically excited metal atoms produced by photoexcitation [39] and gas phase luminescence studies done on other  $\beta$ -diketonate complexes ( $\text{Ni}(\text{hfac})_2$ ,  $\text{Cu}(\text{hfac})_2$ ) have identified bare metal atoms (Ni, Cu) among the products present after 308 nm excitation [14,40].

The luminescence spectra of the photofragments produced upon KrF-excimer laser photolysis at 248 nm of  $\text{Pt}(\text{hfac})_2$  and  $\text{Pd}(\text{hfac})_2$  in the gas phase have been reported [8]. The spectra of the reaction products monitored between 200 and 400 nm show sharp lines attributed to the atomic lines of Pt and Pd protruding from an underlying broad band assumed to be from the parent molecule. The energy dependence of the fluorescence intensities of the Pd atomic lines (330.4, 337.3, and 389.4 nm) is interpreted as an apparent one photon dependence for the dissociation of the parent molecule with an additional photon required for the electronic excitation of the metal atom. Similar results were observed for the Pt atomic lines at 340.8 and 313.9 nm, but the Pt atomic line at 230.8 nm shows a second order increase in the fluorescence intensity with increasing laser energy. Upon increasing the He buffer gas pressure, the atomic fluorescence is not quenched but rather the fluorescence intensity slightly increases. According to the authors, the absence of fluorescence quenching due to collisions with the buffer gas suggests that the initial dissociation of the molecule is through a one photon absorption process and no intermediate states are included. Two photon processes may play a minor part, as shown for the Pt atom fluorescence at 230.8 nm.

#### 4.2.2. Metal-containing molecular fragments

Luminescence spectra of PtC and other photofragments resulting from 308 and 440 nm excitation of  $\text{Pt}(\text{hfac})_2$  at 1 bar and 0.1–10 mbar conditions have been reported [40]. A well-defined vibronic progression with its origin at approximately  $18\,500\text{ cm}^{-1}$  corresponding to the  $\text{A} \rightarrow \text{X}$  transition of PtC was observed under both 440 and 308 nm excitation (Fig. 5). The peaks are clustered into well-defined groups proceeding to lower energy with the most intense members at 540, 572, 608, 649, and 694 nm. These data unambiguously identify PtC as a photoproduct.

Identification of fragments by luminescence spectroscopy is limited to those fragments that are luminescent. Furthermore, association of a specific fragment with specific bands may be difficult (unless the spectrum has been assigned previously). Of importance in this review, luminescence spectra of binary PdC and PdF molecules, which may be formed by gas phase photolysis, have not been reported. An alternative and powerful method, mass spectroscopy, has been used, and results of studies on  $\text{Pd}(\text{hfac})_2$  are reviewed in the following sections.

#### 4.3. Mass spectroscopic identification of photofragments

Intramolecular photofragmentation  $\text{Pd}(\text{hfac})_2$  was studied under the collision-free environment of a molecular beam by using time-of-flight mass spectroscopy. Both visible and UV excitation were used [41]. Extensive fragmentation takes place in one laser pulse with intensities dependent on the excitation frequency. The spectrum

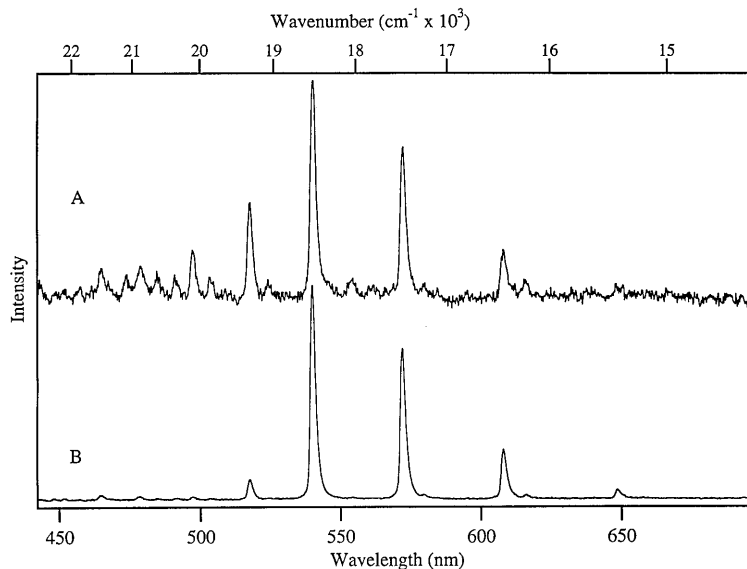


Fig. 5. Emission spectra observed from 440 nm excitation of  $\text{Pt}(\text{hfac})_2$ . (a) Spectrum observed at a pressure of no greater than the vapor pressure of  $\text{Pt}(\text{hfac})_2$ . (b) Spectrum observed using a static chamber with  $\text{Pt}(\text{hfac})_2$  at its vapor pressure with 1 bar Ar buffer.

is dominated by palladium ions; the intensity of the next biggest peak is less than 1/30th that of palladium. The only metal-containing species that are observed are the intact precursor ion and  $\text{PdC}^+$ . Observation of the latter species confirms that the metal carbide is formed in the gas phase. The photoproduction of  $\text{PdC}^+$  has an extremely sensitive wavelength dependence; details of this aspect of the photochemistry are reviewed below.

The ligand undergoes extensive photofragmentation; the most intense signals are from  $\text{C}^+$ ,  $\text{C}_2^+$ ,  $\text{CO}^+$ ,  $\text{CF}^+$ ,  $\text{CF}_2^+$ ,  $\text{CF}_3^+$  and  $\text{C}_2\text{O}^+$  [41]. Also present are the mass signals of some of these fragments with a hydrogen atom attached (for example  $\text{CH}^+$ ,  $\text{C}_2\text{H}^+$ ). Larger ions are also present, such as those that correspond to a metal atom with a full or partial hfac ligand attached as well as the molecular ion. The laser pulse energy effects on the intensity distribution of these fragments are revealing. Power studies show that the processes that lead to the appearance of certain photoproducts are very sensitive to laser fluence conditions. In addition, wavelength dependence studies show that not only the amount but the type of photoproducts generated are sensitive to excitation wavelength throughout the relatively large range where the molecule has its absorption bands. Reaction channels that have different fluence or wavelength dependencies can be identified, and control over the activation of specific reaction channels to produce (or eliminate) specific photoproducts is implied. The important role of these two conditions in the photolytic processes of  $\text{Pd}(\text{hfac})_2$  are discussed in detail in the following sections.



The atomic ions that are observed are indicative of the extensive fragmentation caused by photochemical processes. In some instances, the molecule is atomized down to a single carbon ion. Power dependence studies on the palladium ion confirm that multiphoton processes occur: two or three photon dependencies are observed. These energy considerations, excitation (action) spectra and identification of fragments and products resulting from the photolysis of  $\text{Pd}(\text{hfac})_2$  will help to understand the photolytic pathways that lead to deposition of solids.

#### 4.3.1. *PdC* wavelength dependence

The ratio of  $\text{Pd}^+$  to  $\text{PdC}^+$  is very sensitive to the irradiation wavelength [41]. Changing the wavelength by a few angstroms can cause the formation of  $\text{PdC}^+$  to completely disappear. For example, the  $\text{Pd}^+$  to  $\text{PdC}^+$  ratio is 3:1 with 430 nm excitation but the  $\text{PdC}^+$  is undetectable with 431 nm irradiation.

In order to more completely explore the wavelength dependence of the photofragmentation reaction, mass selected action spectra were obtained. A Nd:YAG pumped optical parametric oscillator provided wavelength tunability throughout the 410–620 nm range with an output of 20 mJ per pulse. The resulting ions were detected using time-of-flight mass spectroscopy. The intensities of the  $\text{Pd}^+$  and the  $\text{PdC}^+$  ions were recorded as a function of the excitation wavelength over a 21 700–23 800  $\text{cm}^{-1}$  excitation region. The action spectra are shown in Fig. 6. Comparison of the two shows that the wavelength dependencies are different. The spectrum obtained by monitoring palladium ions contains sharp peaks that arise from unreported atomic palladium transitions. In contrast, the spectrum obtained while mass monitoring  $\text{PdC}^+$  consists of a broad band with sharp negative-going peaks corresponding to loss of intensity. The formation of  $\text{PdC}^+$  occurs throughout the band and its formation is at a minimum where the  $\text{Pd}^+$  signal is at a maximum. Every ‘hole’ that signifies a loss of  $\text{PdC}^+$  intensity occurs at the wavelength of a sharp resonance from which  $\text{Pd}^+$  is formed efficiently. No wavelengths were found where  $\text{PdC}^+$  is formed without the formation of  $\text{Pd}^+$ . These relationships are most easily observed at the low energy end of the spectra. Between 21 650 and 22 200  $\text{cm}^{-1}$  there are no vibronic bands and both action spectra are smooth. The first significant resonance at 22 220  $\text{cm}^{-1}$  in the spectrum monitoring  $\text{Pd}^+$  (shown by the double-headed arrow in Fig. 6) has a corresponding dip in the spectrum monitoring  $\text{PdC}^+$ . When the intensities of the resonances are large, the dips are saturated. This effect is not yet fully understood.

The formation of  $\text{PdC}^+$  probably involves the binding of the carbon atom of the ligand to the Pd after excitation (Fig. 7). (This alternative binding mode is known for  $\beta$ -diketonate complexes of Pt [42–45].) The high energy excited state accessed by the coherent two-photon absorption may involve a rearrangement involving dissociation of the Pd–O bonds and formation of a Pd–C bond. The excess energy or subsequent absorption would then form  $\text{PdC}^+$  and ligand fragments such as  $\text{CF}_3^+$  that are observed.

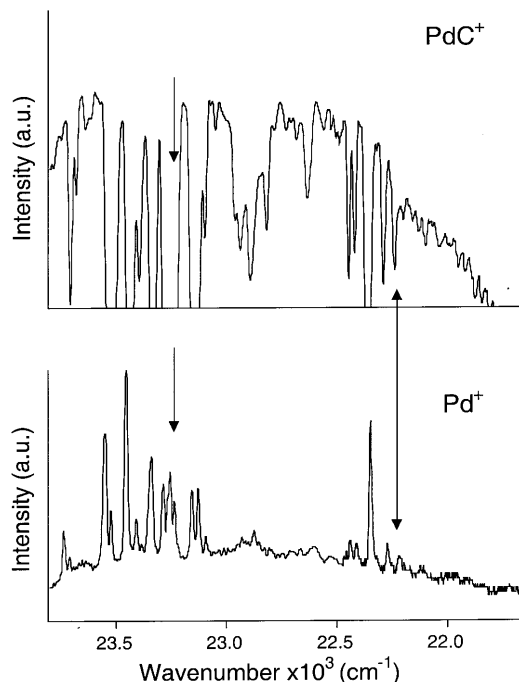


Fig. 6. Action spectra obtained by exciting  $\text{Pd}(\text{hfac})_2$  in a molecular beam between 21 700 and 23 800  $\text{cm}^{-1}$ . The spectra were obtained by monitoring the intensity of  $\text{PdC}^+$  (top) and  $\text{Pd}^+$  (bottom) as a function of the excitation wavelength. The sharp dips (top) and peaks (bottom) occur at wavenumbers when the laser is in resonance with vibronic bands of a ligand-to-metal charge transfer transition in  $\text{Pd}(\text{hfac})_2$ . The double headed arrow indicates the lowest energy resonance and dip discussed in the text. The single arrows show the peak in the  $\text{Pd}^+$  action spectrum and the corresponding dip in the  $\text{PdC}^+$  action spectrum at 431 nm.

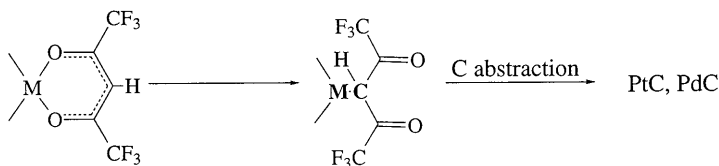


Fig. 7. Proposed intramolecular rearrangements that explain the observed photofragmentation patterns in the mass spectrum and the formation of MC.

## 5. Summary

The excited state properties of the acac and hfac complexes of the two metals that are the subject of this review, palladium and platinum, illustrate the complexities, ambiguities, and opportunities in the field of coordination complexes of  $\beta$ -diketonates. Electronic structure calculations provide insight into the nature of the excited states, but the results are not completely satisfying. The complexes

themselves contribute to the difficulties; the excited states are highly mixed and the energies are highly solvent dependent.

Gas phase spectroscopy and photochemistry provide new and detailed information about the excited states. Photochemistry leads to solid products such as metal films and metal particles. The gas phase photoproducts include metal atoms and small (e.g. diatomic) metal-containing fragments. Interest in the molecules that are precursors for chemical vapor deposition has sparked much of the most recent work.

New experimental techniques are being brought to bear on the excited state processes. Gas phase spectroscopy takes advantage of the absence of inhomogeneous broadening and yields more highly resolved spectra for analysis. The effects of solvents or crystal surroundings can be quantitatively derived. Resonance enhanced multiphoton ionization and mass selection provide a powerful method for obtaining action spectra. This experiment enables excitation spectra, photofragment identification and wavelength dependence of the photoreactivity to be obtained simultaneously.

The lowest excited states of the Pd and Pt hfac complexes involve dd, LMCT and  $\pi\pi^*$  components. In the crystalline environment, the lowest state is primarily LMCT, whereas in the gas phase it is primarily dd. Excitation spectra obtained by monitoring photon emission and ion formation are used to obtain high resolution and assist in assignments. Gas phase laser photolysis leads to ionization, fragmentation and metal deposition. Sensitive wavelength dependencies have been measured for the former two processes. Important progress in understanding the excited state properties is being made, but much remains to be learned.

## Acknowledgements

This work was made possible by a grant from the National Science Foundation (CHE9816552).

## References

- [1] D. Wexler, J.I. Zink, L.W. Tutt, S.R. Lunt, *J. Phys. Chem.* 97 (1993) 13563–13567.
- [2] T.T. Kodas, P.B. Comita, *Acc. Chem. Res.* 23 (1990) 188–194.
- [3] T.H. Baum, C.E. Larson, *Chem. Mater.* 4 (1992) 365–369.
- [4] R.B. Klassen, T.H. Baum, *Organometallics* 8 (1989) 2477–2482.
- [5] T.H. Baum, C.R. Jones, *J. Vac. Sci. Technol. B4* (1986) 1187–1191.
- [6] H.D. Gafney, R.I. Lintvedt, I.S. Jaworowsky, *Inorg. Chem.* 9 (1970) 1728–1733.
- [7] H. Willwohl, J. Wolfrum, *Appl. Surf. Sci.* 54 (1992) 89–94.
- [8] D. Braichotte, C. Garrido, H. van den Bergh, *Appl. Surf. Sci.* 46 (1990) 9–18.
- [9] R.J. Puddephat, *Polyhedron* 13 (1994) 1233–1243.
- [10] V. Bhaskaran, M.J. Hampden-Smith, T.T. Kodas, *Chem. Vapor. Depos.* 3 (1997) 281–286.
- [11] H. Willwohl, J. Wolfrum, V. Zumbach, P. Albers, K. Seibold, *J. Phys. Chem.* 98 (1994) 2242–2247.
- [12] J. Cheon, D.S. Talaga, J.I. Zink, *J. Am. Chem. Soc.* 119 (1997) 163–167.
- [13] D. Wexler, J.I. Zink, *J. Phys. Chem.* 97 (1993) 4903–4909.

- [14] D.S. Talaga, J.I. Zink, *Inorg. Chem.* 35 (1996) 5050–5054.
- [15] J. Cheon, M. Guile, P. Muraoka, J.I. Zink, *Inorg. Chem.* 38 (1999) 2238–2239.
- [16] H.H. Gilgen, *Mat. Res. Soc. Symp. Proc. B* 53 (1984).
- [17] H.S. Cole, Y.S. Liu, J.W. Rose, R. Guida, *Appl. Phys. Lett.* 53 (1988) 2111–2113.
- [18] M.J. Rand, *J. Electrochem. Soc.* 120 (1973) 686–693.
- [19] B. Lecohier, J.M. Philippoz, H. van den Bergh, *J. Vac. Sci. Technol. B* 10 (1992) 262–267.
- [20] R.H. Holm, F.A. Cotton, *J. Am. Chem. Soc.* 80 (1958) 5658–5663.
- [21] F.D. Lewis, G.D. Salvi, D.R. Kanis, M.A. Ratner, *Inorg. Chem.* 32 (1993) 1251–1258.
- [22] C. Reber, J.I. Zink, *Inorg. Chem.* 31 (1992) 2786–2790.
- [23] G.I. Zharkova, I.K. Igumenov, N.M. Tyukalevskaya, *Koord. Khim.* 14 (1998) 67–74.
- [24] S. DiBella, I. Fragala, G. Granozzi, *Inorg. Chem.* 25 (1986) 3997–4003.
- [25] M. Casarin, A. Vittadini, G. Granozzi, I. Fragala, S. DiBella, *Chem. Phys. Lett.* 141 (1987) 193–197.
- [26] D. Wexler, J.I. Zink, *Inorg. Chem.* 35 (1996) 4064–4066.
- [27] R.L. Lintvedt, in: A.W. Adamson, P.D. Fleischauer (Eds.), *Concepts and Models of Inorganic Photochemistry*, Wiley, New York, 1975 (Chapter 7).
- [28] G.T. Behnke, K. Nakamoto, *Inorg. Chem.* 6 (1967) 433.
- [29] M.G. Miles, G.E. Glass, R.S. Tobias, *J. Am. Chem. Soc.* 88 (1966) 5738–5744.
- [30] K. Nakamoto, *Infrared and Raman Spectra of Inorganic and Coordination Compounds*, 4th ed., Wiley, New York, 1986, p. 260.
- [31] K. Nakamoto, Y. Morimoto, A.E. Martell, *J. Phys. Chem.* 66 (1962) 346–348.
- [32] K.V. Kradenov, B.A. Kolesov, G.I. Zharkova, V.G. Isakova, *Zh. Strukt. Khim.* 31 (1988) 56.
- [33] K. Nakamoto, P.J. McCarthy, A. Martell, *J. Am. Chem. Soc.* 83 (1961) 1272–1276.
- [34] I.M. Oglezneva, I.K. Igumenov, *Koord. Khim.* 10 (1984) 313.
- [35] E.J. Heller, *Acc. Chem. Res.* 14 (1981) 368–375.
- [36] E.J. Heller, *J. Chem. Phys.* 68 (1978) 2066–2075.
- [37] Q. Minxin, R. Nonot, H. van den Bergh, *Sci. Sin. Ser. B Eng. Ed.* 27 (1984) 531.
- [38] R.L. Jackson, *Acc. Chem. Res.* 25 (1992) 581–586.
- [39] Z. Karny, R. Naaman, R.N. Zare, *Chem. Phys. Lett.* 59 (1978) 33–37.
- [40] D.S. Talaga, S.D. Hanna, J.I. Zink, *Inorg. Chem.* 37 (1998) 2880–2887.
- [41] P. Muraoka, D. Byun, J.I. Zink, *J. Am. Chem. Soc.* 122 (2000) 1227–1228.
- [42] G.T. Behnke, K. Nakamoto, *Inorg. Chem.* 6 (1967) 440–445.
- [43] F.D. Lewis, A.M. Miller, G.D. Salvi, *Inorg. Chem.* 34 (1995) 3173–3181.
- [44] S. Kimiya, J.K. Kochi, *J. Am. Chem. Soc.* 99 (1977) 11.
- [45] G.C. Dash, R.C. Mishra, D. Panda, B.K. Mohapatra, *Polyhedron* 4 (1985) 1297–1299.